Spatial Coherence and Entanglement of Light

Di Lorenzo Pires, H.

7

Orbital angular momentum spectrum of partially coherent classical beams

In this work we implement a Mach-Zehnder interferometer with an image rotator in one of its arms to measure the orbital angular momentum (OAM) spectrum of a partially coherent beam. By measuring the visibility of the interference as a function of the angle of rotation, the OAM distribution can be recovered via a Fourier transform. Theoretical calculations based on the coherent mode decomposition of the cross-spectral density are in excellent agreement with the experimental data.

H. Di Lorenzo Pires, J. Woudenberg, and M. P. van Exter, *Measurement of the orbital angular momentum spectrum of partially coherent beams*, Opt. Lett. **35**, 889 (2010).

7.1 The OAM spectrum of partially coherent beams

It is well known that light can carry orbital angular momentum (OAM). In particular, coherent beams with an azimuthal phase dependence in the form $e^{il\phi}$, have an OAM of $l\hbar$ per photon [126]. Recently, the concept of OAM was generalized in order to encompass partially coherent light as well [127–131]. One can consider, for instance, beams that can be constructed from an incoherent superposition of Laguerre-Gaussian modes of arbitrary order, but with the same azimuthal index [127, 128]. Serna and Movilla [129] extended the considerations to a more general family of fields, and the relation between the twist of the beam and the OAM was analyzed. However, even in the more typical case of a partially coherent beam that does not transport an overall OAM, we can describe it statistically as a sum of completely coherent beams with a well defined OAM. This description can be formalized by means of the coherent mode decomposition (or Mercer expansion) [3] of the cross-spectral density function $W(\boldsymbol{\rho_1}, \boldsymbol{\rho_2})$ that completely describes the source. For a rotationally symmetric geometry, this decomposition reads

$$W(\boldsymbol{\rho_1}, \boldsymbol{\rho_2}) = \sum_{l=-\infty}^{+\infty} \sum_{p=0}^{\infty} \lambda_{l,p} f_{l,p}(\rho_1) f_{l,p}^*(\rho_2) \frac{e^{il(\phi_1-\phi_2)}}{2\pi}, \tag{7.1}$$

where the transverse position vector $\boldsymbol{\rho} = (\rho\cos\phi, \rho\sin\phi)$ is written in polar coordinates. This representation is very fundamental, being equivalent to a matrix diagonalization or the search for the eigenvalues $\lambda_{l,p}$ and the eigenfunctions $f_{l,p}(\rho)$. Physically, it reveals the modal structure of the source and $\lambda_{l,p}$ can be interpreted as the probability of finding a coherent mode $f_{l,p}$. The larger the number of modes present, the more incoherent is the source. This implies that Eq. (7.1) would contain only one term for a completely coherent (e.g. a laser) beam. This decomposition is also crucial to OAM analysis of partially coherent light [129, 132] and allows us to assign a probability $P_l = \sum_p \lambda_{l,p}$ of having a mode with OAM $l\hbar$.

The distribution of the probabilities P_l is known as the OAM spectrum of the beam. To the best of our knowledge, no measurements of this spectrum for partially coherent light have been reported so far. In this Chapter we will present such an experiment. We will implement an approximately quasi-homogeneous light source [133], justifying the expansion in Eq. (7.1). The intrinsic symmetry $P_l = P_{-l}$ implies that the beam carries no overall OAM. Generalizations will be discussed at the end of this Chapter.

7.2 Experiments and discussions

Figure 7.1 shows the experimental setup used to generate a partially coherent beam and to measure its OAM spectrum. A $15\times$ magnified image of a light emitting diode (LED) is made on an adjustable circular aperture of diameter d_1, after being filtered by a polarizer. We can regard this aperture as an incoherent, circular source of uniform intensity. The light propagates a distance L to a second

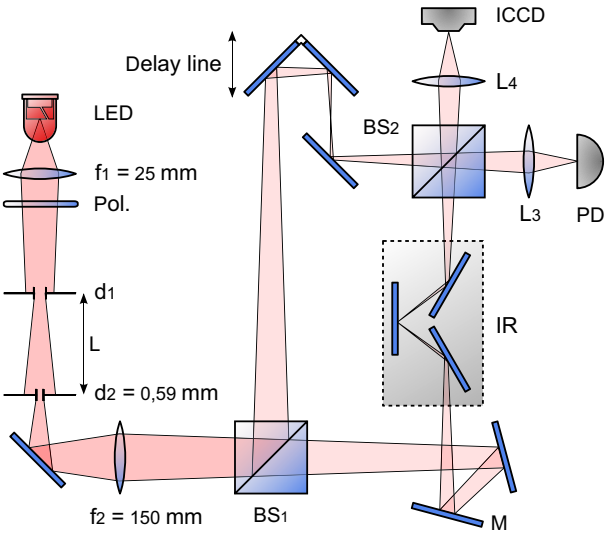

Figure 7.1: Experimental setup used to create a partially coherent beam and to measure its OAM spectrum. See details in the text.

circular aperture of fixed diameter d_2. Using the van Cittert-Zernike theorem [2], the cross-spectral density of the beam just after the second aperture is given by

$$W(\boldsymbol{\rho_1}, \boldsymbol{\rho_2}) = T(\rho_1)T(\rho_2)\frac{J_1(\alpha|\boldsymbol{\rho_1} - \boldsymbol{\rho_2}|)}{\alpha|\boldsymbol{\rho_1} - \boldsymbol{\rho_2}|}e^{\frac{i\pi}{\lambda L}(\rho_1^2 - \rho_2^2)}, \tag{7.2}$$

where $T(\rho)$ is the transmission function of the second aperture, $J_1(\rho)$ is a Bessel function of the first kind, and $\alpha = \pi d_1/\lambda L$. The wavelength λ is defined by spectral filters in front of our detection units, which are centered at 826 nm and have 2 nm bandwidth.

From Eq. (7.2), the P_l distribution can be analytically calculated. The Gegenbauer theorem [134] can be used to separate the radial and angular dependence of the term containing the Bessel function in Eq. (7.2), which can then be written in a series of functions of ρ_1 and ρ_2 times $e^{il(\phi_1 - \phi_2)}$. Omitting the details, we can integrate out the modulus squared of the radial dependence and express the OAM spectrum, apart from a global normalization factor, as

$$\begin{aligned} P_l = &\sum_{i=0}^{k}\sum_{j=0}^{k}(1 + |l| + 2i)(1 + |l| + 2j) \\ &\times \left[\mathbb{H}(\alpha d_2/2, 1 + |l| + 2i, 1 + |l| + 2j)\right]^2, \end{aligned} \tag{7.3}$$

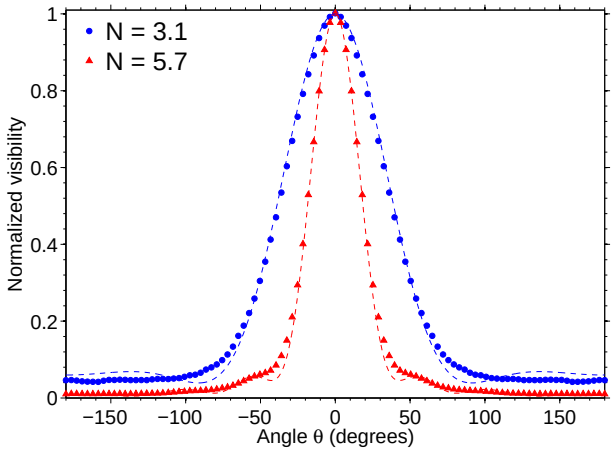

Figure 7.2: Measured visibility $V(\theta)$ for two different circular apertures. The circles corresponds to a diameter $d_1 = 1.2$ mm ($N = 3.1$) and the triangles to $d_1 = 2.2$ mm ($N = 5.7$). The dashed lines are the theoretical curves, calculated by substituting P_l from Eq. (7.3) in Eq. (7.5).

where the function $\mathbb{H}$ is defined as

$$\mathbb{H}(\gamma, m, n) = \frac{2^{-m-n}\gamma^{m+n}}{m!n!(m+n)}\ {}_2F_3\left[\left\{\frac{m+n}{2}, \frac{m+n+1}{2}\right\}, \{1+m, 1+n, 1+m+n\}, -\gamma^2\right], \tag{7.4}$$

and ${}_2F_3$ is a generalized hypergeometric function [135]. The summations in Eq. (7.3), which are associated with the radial mode index p, go in principle up to $k = +\infty$, but numerically, using $k = 5$ gives an error less than 0.5% for our particular values. We see from Eq. (7.3) that the generated sources can be conveniently characterized by a single, dimensionless Fresnel-type number $N = \pi d_1 d_2/4\lambda L$. For our geometry with $L = 21$ cm, $\lambda = 826$ nm, and fixed $d_2 = 0.59$ mm, the investigated apertures $d_1 = 1.2$ mm and $d_1 = 2.2$ mm correspond to $N = 3.1$ and $N = 5.7$.

In order to measure the P_l distribution, we implement an apparatus similar to the one theoretically proposed by Zambrini and Barnett [136]. The generated beam is sent through a Mach-Zehnder interferometer, where it is initially split in beam splitter BS1 and then recombined at BS2. In one of the arms of this interferometer there is an image rotator (IR), which rotates the input image by θ degrees around its axis. A $f = 150$ mm lens makes a $4\times$ magnified image of the second aperture in the center of the IR. A delay line allows us to set both arms of the interferometer to the same length. All the light in one of output ports of BS2 is collected with lens L3 and focused on the active area of a photodiode (PD).

We can summarize the effect of the interferometer as follows. Consider first a pure (coherent) beam with OAM$= l\hbar$. Light that goes through the lower arm of the interferometer will acquire a phase $e^{il\theta}$ due to an image ro-

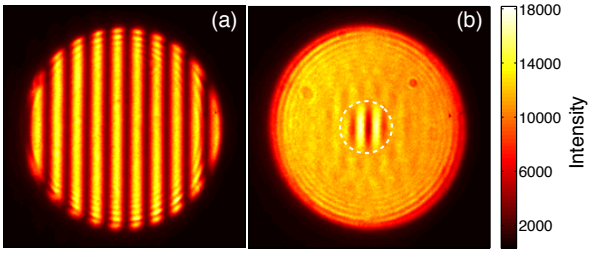

Figure 7.3: Measured interference pattern for (a) $\theta = 0^\circ$ and (b) $\theta = 180^\circ$. Beam splitter BS2 was on purpose misaligned in order to allow the visualization of vertical fringes. The dashed line delimits the theoretical coherence area.

tation of θ and $e^{i\delta}$ due to a small displacement of the piezo-controlled mirror M. The intensity of the recombined beams as measured by the PD is then $I \propto |e^{i\phi} + e^{i(\phi+l\theta+\delta)}|^2 \propto 1 + \cos(l\theta + \delta)$. For an incoherent superposition of beams with OAM$= l\hbar$ with probability P_l (satisfying $P_l = P_{-l}$), the intensity measured is then $I \propto 1 + V(\theta)\cos\delta$, where the visibility of the total interference

$$V(\theta) = \sum_{l=-\infty}^{l=+\infty} P_l \cos(l\theta) \tag{7.5}$$

can be measured in the standard way, by producing small displacements with mirror M and calculating $V = (I_{max} - I_{min})/(I_{max} + I_{min})$. The OAM spectrum P_l can thus be recovered by measuring $V(\theta)$ and numerically performing an inverse Fourier transform. For $\theta = 0^\circ$, the visibility should be theoretically $V = 100\%$. Experimentally we obtain $V = 90\%$. We attribute this discrepancy to an almost unavoidable non-perfect overlap of the phase fronts at the BS2. All our results will be normalized to account for this effect.

Figure 7.2 shows the measured visibility $V(\theta)$ for two different diameters d_1 of the first aperture. We see that a smaller aperture leads to a broader visibility curve, in agreement with the theoretical curves.

The physical reason why the visibility decreases with rotation can be visualized in Fig. 7.3. We now misalign BS2, so that fringes can be observed, and record the interference pattern with an intensified CCD camera (ICCD). Figure 7.3(a) shows the measured pattern for $\theta = 0^\circ$ and Fig. 7.3(b) for $\theta = 180^\circ$. When we superpose the rotated field, points with a larger radius suffer also a larger linear displacement $|\boldsymbol{\rho_1} - \boldsymbol{\rho_2}| = 2\rho\sin(\theta/2)$. The lack of spatial coherence between these points leads to a decreased fringe visibility. We see that the visibility of the interference remains high within a certain radius, which is related to the coherence length of the field. This is confirmed by plotting in Fig. 7.3(b) the theoretical boundaries of the coherence area, as defined by the first zero of Eq. (7.2). Figure 7.3(b) thus provides a direct visualization of the spatial coherence of the source.

Figure 7.4 shows the OAM spectrum obtained by numerically Fourier trans-

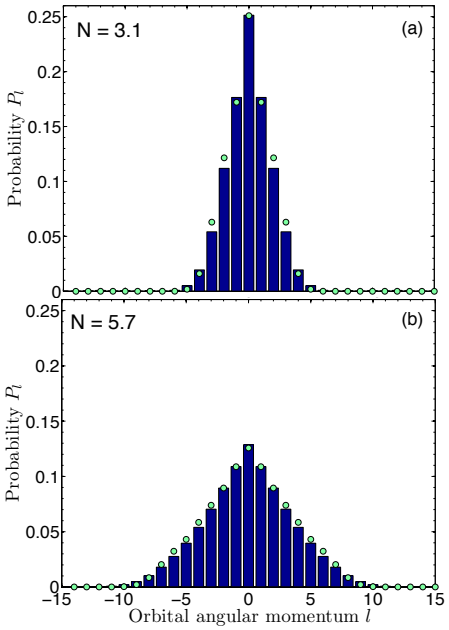

Figure 7.4: OAM spectrum obtained for two different circular apertures (a) $d_1 = 1.2$ mm ($N = 3.1$) and (b) $d_1 = 2.2$ mm ($N = 5.7$). The bars represent the experimental results and the circles the theoretical predictions, according to Eqs. (7.3) *and* (7.4).

forming the visibilities in Fig. 7.2. The bars represent the experimental results and the circles the theoretical predictions according to Eqs. (7.3) and (7.4). The weights P_l represent, as before, the probability of having a mode in an OAM eigenstate with azimuthal number l. Notice the very good agreement between theory and experiment. We can see that the P_l distributions have an approximately triangular shape and a well defined cutoff, associated with the sharp edges of the two apertures. This cutoff is higher for a system with a larger aperture; for an aperture with diameter $d_1 = 1.2$ mm, we have $|l_{max}| = 5$ while for $d_1 = 2.2$ mm, the number of modes is limited by $|l_{max}| = 10$.

It is a well known result in classical optics that the number of available spatial channels in a certain optical system can be (approximately) quantified by the "degrees of freedom" or Shannon number S of this system [137], which is proportional to $A\Omega/\lambda^2$. Here A is the area of the first aperture and Ω the solid angle subtended by the second aperture. More spatial modes are clearly allowed in a system with larger apertures. In our experiments, only the azimuthal modes, and not the radial ones, are being counted. This justifies the dependence of our results on the Fresnel-type number $N = \sqrt{S}$.

7.3 Conclusion

In conclusion, we presented the first experimental measurement of the OAM spectrum of a partially coherent light. Our source was designed to be approximately quasi homogeneous, without an overall OAM. The experimental technique can be extended to more general beams. If the symmetry $P_l = P_{-l}$ is not obeyed, the phase of the interferometer should be stabilized and the intensity difference of the two output beams should be measured instead [136]. An additional measurement with a $\pi/2$ phase shift will provide the amplitude of a *sine* series that should now be added to Eq. (7.5). Furthermore, this extended method also works for asymmetric beams or apertures [136]. Be aware, however, that due to the *quasi-intrinsic* nature of the OAM, the spectrum P_l will depend on the choice of the rotation axis.